



Investigation new positions for catalytic activity of *Chaetomium thermophilum* and *Ceriporiopsis subvermispota* formate dehydrogenases

Kübra Koçdemir, Fatma Şen, Yasin Adem Wedajo, Muazzez Çağla Bilgici, Mustafa Bayram, İlke Selçuk, Berin Yilmazer, Mehmet Mervan Çakar, Elif Sibel Aslan & Barış Binay

To cite this article: Kübra Koçdemir, Fatma Şen, Yasin Adem Wedajo, Muazzez Çağla Bilgici, Mustafa Bayram, İlke Selçuk, Berin Yilmazer, Mehmet Mervan Çakar, Elif Sibel Aslan & Barış Binay (2020): Investigation new positions for catalytic activity of *Chaetomium thermophilum* and *Ceriporiopsis subvermispota* formate dehydrogenases, Biocatalysis and Biotransformation, DOI: [10.1080/10242422.2020.1863951](https://doi.org/10.1080/10242422.2020.1863951)

To link to this article: <https://doi.org/10.1080/10242422.2020.1863951>



View supplementary material [↗](#)



Published online: 23 Dec 2020.



Submit your article to this journal [↗](#)



Article views: 114



View related articles [↗](#)



View Crossmark data [↗](#)

RESEARCH ARTICLE



Investigation new positions for catalytic activity of *Chaetomium thermophilum* and *Ceriporiopsis subvermispota* formate dehydrogenases

Kübra Koçdemir^{a*}, Fatma Şen^{a*}, Yasin Adem Wedajo^b, Muazzez Çağla Bilgici^c, Mustafa Bayram^c, İlke Selçuk^a, Berin Yılmaz^a, Mehmet Mervan Çakar^a, Elif Sibel Aslan^d and Barış Binay^e

^aDepartment of Molecular Biology and Genetics, Gebze Technical University, Gebze, Kocaeli, Turkey; ^bDepartment of Chemistry, Gebze Technical University, Gebze, Kocaeli, Turkey; ^cDepartment of Biotechnology, Gebze Technical University, Gebze, Kocaeli, Turkey; ^dDepartment of Molecular Biology and Genetics, Biruni University, Topkapı, İstanbul, Turkey; ^eDepartment of Bioengineering, Gebze Technical University, Gebze, Kocaeli, Turkey

ABSTRACT

NAD⁺-dependent formate dehydrogenases (FDHs, E.C 1.2.1.2) catalyse the reversible reaction of CO₂ to formate ion (HCOO⁻) and reduces NAD⁺ molecule to NADH. Previously described FDHs from *Chaetomium thermophilum* (CtFDH) and *Ceriporiopsis subvermispota* (CsFDH) are active against formate and HCO₃⁻. In this study, we examined the functional effects of active site mutations in Ct and Cs NAD⁺-dependent FDHs. The residues Ile94, Asn120, Val310, His312 at CtFDH and Asn312, Val313, Val331 at CsFDH are located in the active site. The effects of amino acid changes on catalytic properties and thermal stability of CtFDH and CsFDH revealed some interesting results compared with structurally equivalent positions that have been studied in the literature. The strongest effect was observed in CsFDH Val313Pro against HCO₃⁻. The K_M value of the CsFDH Val313 enzyme for HCO₃⁻ substrate dramatically decreased, and enzyme activity increased. In CtFDH mutants, all enzymes except Val310Asn showed an increased k_{cat} value when K_M values increase. Analyses of results of mutant CtFDHs and CsFDHs give some promising results for CO₂ reduction as compared to the literature. Structural analyses of the substrate-binding site were done by homology modelling.

ARTICLE HISTORY

Received 3 November 2020
Revised 8 December 2020
Accepted 9 December 2020

KEYWORDS

Protein engineering; NAD⁺-dependent formate dehydrogenase; CO₂ reduction; site-directed mutagenesis; molecular modelling

Introduction

NAD⁺-dependent formate dehydrogenases (FDHs) (E.C 1.2.1.2) catalyse formate oxidation to carbon dioxide (CO₂) by the reduction of NAD⁺ to NADH (Tishkov and Popov 2004). In a formate oxidation reaction, a single carbon-hydrogen bond is broken in the formate and a new carbon-hydrogen bond is formed in the NADH, producing CO₂ (Schiøtt et al. 1998). NAD⁺-dependent FDHs are mostly seen in industrial regeneration systems, where they are usually used for the synthesis of valuable optically active chiral compounds such as drugs and amino acids (Hatrongjit and Packdibamrung 2010). Among the enzymes used for cofactor regeneration, formate dehydrogenase has been reported as the most suitable due to having many advantages in the recycling process of NADH: an appropriate thermodynamic equilibrium, the immobility of the substrate, and an inert by-product (CO₂).


Since the formed CO₂ can be easily removed from the reaction environment, NADH is obtained purely. Until now, FDHs have been evaluated only as excellent NADH regenerators, although recent studies have shown that some FDHs have the ability to reduce carbon dioxide to formate as a reverse reaction (Lu et al. 2006, Alissandratos et al. 2013, Aslan et al. 2017, Pala et al. 2018).

Increased atmospheric CO₂-concentration is widely being considered the main driving factor of global warming (Florides and Christodoulides 2009). Increases in human population, industrial activity, and natural disasters (volcanic eruptions, etc.) are the major causes of CO₂ emission (Çakar et al. 2020). Climate change is a global challenge that has no borders; coordinated work by all countries is required to combat it (Glueck et al. 2010). It has been predicted that by 2050 the CO₂ concentration in the atmosphere will reach over 500 ppm, nearly double the concentration present

CONTACT Barış Binay  binay@gtu.edu.tr

*These authors contributed equally.

This article has been republished with minor changes. These changes do not impact the academic content of the article.

 Supplemental data for this article can be accessed [here](#).

© 2020 Informa UK Limited, trading as Taylor & Francis Group

before the industrial revolution (280 ppm) (Yuan et al. 2019). Biotransformation of CO₂ has the benefit of global warming reduction and also is a powerful alternative to produce renewable energy (Çakar et al. 2020). Because of the ability of biocatalysts to efficiently catalyse processes under mild conditions with limited by-product formation, they play a critical role in the transformation of CO₂ by lowering activation barriers (Alissandratos et al. 2013, Choe et al. 2014). However, only a few biocatalysts, such as formate dehydrogenase, can capture CO₂. The reverse reaction of FDHs has promising potential for methods of carbon fixation from the atmosphere and the oceans. Formate, which can be produced from CO₂ as a feedstock, is also an economically and environmentally valuable chemical (Alissandratos et al. 2013, 2014, Hawkins et al. 2013).

Our previous results showed that NAD⁺/NADH-dependent FDHs show low catalytic efficiency for the reduction of CO₂ (Aslan et al. 2017). Also, regeneration of cofactors requires that FDHs have stability in extreme process conditions and high cofactor turnover rates. However, the reported FDHs have limited properties such as thermostability and catalytic efficiency in order to fulfil the industrial requirements (Labrou and Rigden 2001, Galkin et al. 2002, Leopoldini et al. 2008, Alissandratos et al. 2013, Wu et al. 2013, Bassegoda et al. 2014, Choe et al. 2014, Aslan et al. 2017, Maia et al. 2017). These enzymes would need to be engineered before they could be used at an industrial scale for the conversion of CO₂ to hydrocarbons and to have more efficient cofactor regeneration. For protein engineering improvements, study of the structure–function relationships at the FDH active site, and especially the catalytic mechanism, is essential.

Although FDH enzymes have conserved amino acid positions that form as catalytic sites, they reveal different kinetic rates for the same substrate (Tishkov and Popov 2004). Single-amino acid changes in the active sites of enzymes can significantly alter the stability, catalytic efficiency, and substrate specificity of the enzyme (Karimäki et al. 2004, Kim et al. 2014, Lenz et al. 2018). Therefore, we investigated how specific mutations could affect the kinetic properties of FDH enzyme. In order to examine the catalytic site of CsFDH, it was aligned with well-known FDHs and three non-aligned positions were selected for mutation based on their relative proximity to the active site. CtFDH also has one of these three amino acid substitutions which is Thr to Val substitution on the same position. Although CsFDH and CtFDH have shown quite different catalytic characteristics as stated in previous studies (Aslan et al. 2017), the common

substitution makes this position worth to investigate. Also, previously identified three significant residues (Çakar et al. 2020, Yilmazer et al. 2020) were selected for the alanine scanning mutagenesis in order to support previous studies. For this purpose, desired mutations were introduced into the active site of the FDHs from Cs and Ct. The kinetic parameters were determined, and the results were investigated with homology modelling and enzyme–substrate/cofactor docking studies to provide a further understanding of the forward and reverse catalytic mechanism of the FDHs.

Materials and methods

General equipment and chemicals

All chemicals were purchased from Sigma-Aldrich. DH5a competent cells, BL21 competent cells, and the pET 45b (+) plasmid were purchased from Sigma Aldrich and the 6xHis-tag protein purification column was a BabyBio purchased from BioWorks. The site-directed mutagenesis was carried out under PCR with a Techne Prime Thermal Cycler purchased from Techne. The plasmid isolation kit was purchased from NucleoSpin Plasmid (NoLid), and a mini kit for plasmid DNA purification was purchased from Macherey-Nagel. The centrifuge was Beckman Coulter purchased from Sigma, and the benchtop centrifuge was purchased from Allegra. The gel-screening blue light was from Serva, and the absorbance microplate reader and microplate spectrometer Epoch2 was purchased from BioTek.

Bioinformatic analysis

The CsFDH was aligned with well-known FDHs and three non-aligned residues were selected for mutation based on their relative proximity to the active site (Figure 1). The three candidates, Asn312, Val313, and Val331 residues in 2NAD numbering that close to the active site, were identified. The crystal structures of CtFDH (PDB:6T8Y) and previous studies were used as a guide to the selection of CtFDH. Previously identified Ile94, Asn120 and His312 residues were selected for Alanine substitution. The oligonucleotide primers were to confer the desired mutations in the CtFDH and CsFDH plasmids.

Improving the purification of CsFDH and CtFDH

The desired mutations were incorporated by an overlapping polymerase chain reaction (PCR) method using



Figure 1. Alignment of formate dehydrogenases. Symbols: Ps, *Pseudomonas* sp. (strain 101) (PseFDH); Cb, *Candida boidinii* (CbFDH); Ts, *Thiobacillus* sp. (strain KNK65MA) (TsFDH); Cm, *Candida methylca* (CmFDH); Ct, *Chaetomium thermophilum* (CtFDH).

Table 1. List of primers used for site-directed mutagenesis.

Source of FDH	Name	Sequence (5' to 3')
Ct	Ile94Ala_fw	ACTGGCGGTGACCGCCGGTGCCGGCAGCGATCAT
	Asn120Ala_fw	GCTGGTTAATACGGCGCCGGCGCTATCGTCGTG
	Val310Asn_fw	GTGGCAATGCTATGAACCCGCACATGAGCG
	His312Ala_fw	GGCAATGCTATGGTACCGGCATGAGCGGCACCA
	Val310Thr_fw	GGTGGCAATGCTATGACCCCGCAGATGAGCG
Cs	Asn312Phe_fw	GCAGGCGATGTGTGGTTTGTTCAGCCGGCG
	Val313Pro_fw	GGCGATGTGTGGAATCCGCAGCCGGCGC
	Val331Thr_fw	GTGGCAATGGTATGACCCCGCACTATAGCG

complementary oligonucleotides. Primers ordered from Eurofins and their sequences are listed in Table 1. The wild-type CtFDH and CsFDH genes were subjected to site-directed mutagenesis according to the standard PCR method (98 °C for 30 seconds, 98 °C for 10 seconds, 65 °C for 20 seconds, 72 °C for 2.5 minutes, 72 °C for 7 minutes for the final extension for one cycle) in the presence of 1 µL dNTPs mix, 2.5 µL primer mix, 0.5 µL Phusion High Fidelity DNA polymerase in a total 50 µL reaction. The amplified PCR product involves 6xHis-tag at the C-terminal and N-terminal of the pET45b (+) expression plasmid. After PCR, 1 µL of the *DpnI* restriction enzyme was added into the PCR product and incubated at 37 °C for 2 hours. *DpnI*-treated PCR products were confirmed on 1% agarose gel electrophoresis. The mutated product was transformed into *E. coli* DH5α competent cells for gene cloning and selected on Luria-Broth (LB) agar containing 100 µg/ml ampicillin. The final constructed product was sequenced in Eurofins MWG Operon. All of the mutation positions progressed under the same cloning and mutation procedure as described.

Expression and purification of Wild-Type and mutant recombinant CtFDH and CsFDH proteins

The obtained and confirmed mutant and wild type CtFDH and CsFDH genes were expressed in *E. coli* BL21 (DE3) cells for the production and purification of the corresponding proteins. Bacterial cultures involving the desired plasmid, which was transformed in *E.*

coli BL21 protein expression vectors, were grown overnight (16–18 h) on a rotary shaker in LB (~10–15 mL) supplemented with ampicillin (100 µg/mL). Previously prepared Studier Media (autoinduction) involved 4 mL LB media containing the culture and 100 µg/mL ampicillin incubated overnight (16 h) on a rotary shaker (Studier 2005). After that, the cells were harvested by centrifugation (15,000 × g, 20 min, +4 °C), and the resulting cell pellet was stored at –80 °C.

The wild type and mutated proteins were purified by His-tag affinity column using nickel nitrilotriacetic acid (Ni-NTA) resin (supplied with the kit). The pelleted cells were kept at 37 °C for 30 min and then resuspended in 10 mL of buffer A containing 20 mM NaH₂PO₄, 500 mM NaCl and 30 mM imidazole, with the pH adjusted to 7.4. Lysozyme (1 mg/mL) was added to the cell suspension, PMSF (phenylmethylsulfonyl fluoride, 4 µL/g) was added to the cell suspension and the resulting mixture was incubated on ice for 30 min. Each incubated pellet was sonicated to break up the cells to obtain extracellular extract for further purification studies. A sample (50 µL) was collected at each step to determine the total protein content. The remaining cell suspension was centrifuged at 15,000 × g for 15 min at 4 °C.

The 6xHis-tag proteins were purified on Ni-NTA HisTrap column chromatography using a linear gradient of 50–250 mM imidazole in a buffer consisting of 200 mM sodium phosphate buffer (NaPi), 500 mM NaCl pH 7.4. The fractions were analysed with sodium

dodecyl sulphate-polyacrylamide gel electrophoresis (SDS-PAGE). Purified proteins were concentrated with 30 kDa cut-off ultracentrifuge filter tubes. The purified proteins were quantitated with the bicinchoninic acid assay (Smith et al. 1985).

pH assay

The relative activity of wild type and all the mutant FDHs were measured in different 100 mM buffers for different pH ranges at 25 °C in a solution containing 10 mM formic acid buffer and 1.0 mM NAD⁺. The selected 100 mM buffers were citrate for pH 3.0–6.0, NaPi for pH 6.0–7.5, Tris-HCl for pH 7.5–9.0, Glycine for pH 9.0–10.0, sodium carbonate pH 9.5–11.0 and KCl-NaOH pH 11.0–13.0.

Thermostability assay

The thermostability of enzymes was measured by incubating the purified FDHs for 15 min at temperatures from 25 °C to 65 °C. The residual activity of the incubated samples was measured in specific activity assays at 24 °C. The specific activity of FDHs was measured in optimum 100 mM buffers containing 20 mM sodium formate and 1.0 mM NAD⁺ for formate oxidation or 20 mM sodium bicarbonate and 0.5 mM NADH for CO₂ reduction.

Enzyme kinetic assays

Kinetic parameters of wild type and all the mutant FDHs were determined through monitoring the change in absorbance at 340 nm due to NADH formation or consumption in 100 mM of optimum buffers for each FDH. The reaction mixtures contained sodium formate and 1.0 mM NAD⁺ for formate oxidation and sodium bicarbonate and 0.5 mM NADH for CO₂ reduction. The substrate concentration ranges for the different assays were 0.5–50 mM for formate, 0.5–40 mM for sodium bicarbonate. All reactions were performed at 25 °C. The Michaelis-Menten kinetic constants were determined from triplicate measurements of the initial velocities using GraphPad Prism software.

Molecular modelling

The 3D homology model of CsFDH was generated in Swiss-Model (Arnold et al. 2006) using the published structure of *Pseudomonas sp. 101* formate dehydrogenase (PseFDH, PDB ID: 2NAD) (Lamzin et al. 1994) as a template, and the published structure was used for

CtFDH (PDB ID: 6T8Y) (Yilmazer et al. 2020). Formate and hydrogen carbonate substrates were docked into CsFDH and CtFDH (hydrogen carbonate only) active site pockets *in silico* via the AutoDock Vina (Trott and Olson 2010). Substrate binding pocket drawings were done by PyMOL (Molecular Graphics System, Version 2.0 Schrodinger, LLC), 2D cofactor binding domain drawings were done by PoseView (Stierand and Rarey 2010), and rotamers of mutated positions were predicted with UCSF Chimera (Pettersen et al. 2004, Shapovalov and Dunbrack Jr. 2011).

Results and discussion

Expression and purification

Site-directed mutagenesis was used to construct mutations at selected positions in the CtFDH and CsFDH genes. The desired mutations were confirmed by DNA sequencing. FDH protein variants containing the N-terminal 6xHis-tag were isolated by Ni-NTA HisTrap column chromatography. The fractions were analysed with SDS-PAGE (Supplementary Figure S1) and pure fractions were collected. Wild-type and the mutant enzymes were obtained with high yield.

pH and thermostability

The relative thermostability of the enzymes was calculated by the ratio of initial rate constants of wild-type and the mutants (Tables 2 and 3). The initial rate constant derived from inactivation rate constant which is used to determine thermal stability. The dependency of the inactivation rate constant is determined by transition state theory (Tishkov and Popov 2006). The relative thermal stability is determined by the ratio of initial rate constants for the initial enzyme and its

Table 2. Relative thermostability of CtFDH mutants against formate and hydrogen carbonate^a.

Temperature (°C)	Substrates					
	Formate				Hydrogen carbonate	
	Ct I94A	Ct V310N	Ct V310T	Ct H312A	Ct I94A	Ct V310N
25	2.6	4.8	4.6	2.5	6.5	7.3
30	1.0	5.4	5.8	2.2	5.2	8.8
35	0.5	1.9	4.6	2.1	0.9	7.9
40	2.0	1.5	4.0	1.6	0.5	1.8
45	2.9	1.7	4.6	1.2	2.1	6.6
50	4.8	1.3	2.7	1.3	5.7	6.7
55	3.3	3.2	0.3	1.2	5.9	6.7
60	0	0	2.9	0	0	0
65	0	0	2.9	0	0	0

^aThe initial rate constants that used for thermal stability calculation are wild type enzyme measured at 55 °C against formate and at 40 °C for CO₂ reduction.

mutant ($k_{in}^{ini}/k_{in}^{mut}$). Due to their direct relation to the activities, the lower values indicate more stable enzymes.

Rate constants of wild-type enzymes were measured at 55 °C in forward reaction (formate oxidation) and 40 °C against HCO_3^- for the CtFDH wild-type, while it was measured at 45 °C in forward reaction and 30 °C against HCO_3^- for the CsFDH wild-type. In the formate-direction reaction, the CtFDH-Val310Thr mutant is more stabilized than the wild-type at 55 °C and CtFDH-Ile94Ala mutant is more stabilized than wild-type at 35 °C, whereas other mutants did not show any significant difference. At 35 °C, CsFDH-Asn312Phe mutants were more stable in formate oxidation than the wild-type, but drastically lost stability in CO_2 reduction. The stability of the CtFDH-Ile94Ala mutant was increased at 35 °C and 40 °C against HCO_3^- , while CtFDH-Val310Asn mutants showed lower stability than the wild-type. The Val313Pro mutant was also more stabilized than its wild-type at 35 °C against HCO_3^- .

Table 3. Relative thermostability of CsFDH mutants against formate and hydrogen carbonate^a.

Temperature (°C)	Substrates				
	Formate			Hydrogen carbonate	
	Cs N312F	Cs V313P	Cs V331T	Cs N312F	Cs V313P
25	1.8	6.2	1.5	10.3	2.2
30	1.0	6.1	1.5	2.4	1.0
35	0.9	5.8	1.3	4.6	0.8
40	2.7	5.3	1.1	5.5	1.7
45	28.5	4.6	1.2	11.9	1.9
50	211	4.1	3.8	10.7	2.1
55	0	24.8	19.2	30.8	5.1
60	0	46.9	97.4	0	0
65	0	0	0	0	0

^aThe initial rate constants that used for thermal stability calculation are wild type enzyme measured at 45 °C for formate oxidation and at 30 °C for CO_2 reduction.

The optimum pH rates of CsFDH, CtFDH, and their mutants for formate oxidation and CO_2 reduction are shown in Table 4. The measurements show that the optimum pH for formate oxidation is 6.5 for the wild-type, Asn312Phe and Val313Pro mutants, whereas 6.0 is the pH optimum for the Val331Thr mutant of CsFDH. The Val331Thr mutant showed higher activity towards formate than the wild-type CsFDH between pH 6.0–10.0. Although they show similar patterns between pH 6.0 and 10.0, the formate oxidation activity of the mutant is higher than the wild type in acidic pH (4.5, 5.0). On the other hand, no significant differences in pH optimum were found for the CsFDH-Val313Pro and CsFDH-Asn312Phe mutants. The optimum pH for formate oxidation is 7.0 for the wild-type CtFDH and His312Ala, whereas the optimum pH is 7.5, 5.5, and 5.0 for the Ile94Ala, Val310Asn and Val310Thr mutants, respectively. While wild-type CtFDH and His312Ala show similar patterns, the mutant has a slightly higher activity for formate oxidation. CtFDH-Val310Asn shows higher activity than wild type CtFDH in acidic pH (5.0–7.0), while formate oxidation in CtFDH-Ile94Ala is slightly higher in neutral pH.

The measurements show that the optimum pH of activity towards HCO_3^- is 6.0 for the wild-type CsFDH, 7.0 for Asn312Phe, and 6.5 for Val313Pro mutants. Even though the wild-type and mutants show similar patterns, the Asn312Phe mutant has lower CO_2 reduction activity than the wild-type. The optimum pH towards HCO_3^- is 8.0 for the wild-type CtFDH, whereas for the Ile94Ala and Val310Asn mutants, the optimum pH is 6.0. Both CtFDH mutants show slightly higher activity than wild-type in acidic pH (5.0–6.0).

Enzyme kinetic assays

Site-directed mutagenesis at non-conserved amino acid positions in the active site was used to explore

Table 4. The kinetic constants of CtFDH and CsFDH wild type and mutant for hydrogen carbonate and formate.

CtFDH	Substrate							
	Formate				Hydrogen carbonate			
	Optimum pH	k_{cat} (s^{-1})	K_M (mM)	k_{cat}/K_M ($s^{-1}mM^{-1}$)	Optimum pH	k_{cat} (s^{-1})	K_M (mM)	k_{cat}/K_M ($s^{-1}mM^{-1}$)
Wild-Type	7.0	1.5 ± 0.001	3.22 ± 0.460	0.465 ± 0.002	8	0.023 ± 0.000	0.32 ± 0.070	0.0690
Ile94Ala	7.5	0.233 ± 0.008	20.85 ± 1.49	0.011 ± 0.00	6	0.191 ± 0.1	1.734 ± 0.9	0.110 ± 0.11
Asn120Ala			^a		7.5	0.173 ± 0.01	0.95 ± 0.02	0.164 ± 0.01
Val310Asn	5.5	0.136 ± 0.009	1.58 ± 0.69	0.086 ± 0.013	6	0.091 ± 0.005	1.25 ± 0.403	0.072 ± 0.012
His312Ala	7	0.100 ± 0.000	7.68 ± 0.56	0.013 ± 0.000			^a	
Val310Thr	5	0.387 ± 0.028	6.80 ± 1.90	0.057 ± 0.014			^a	
CsFDH								
Wild-Type	6.5	0.554 ± 0.008	5.20 ± 0.630	0.107 ± 0.007	6	0.011 ± 0.001	14.46 ± 6.97	0.001 ± 0.000
Asn312Phe	6.5	0.254 ± 0.007	4.126 ± 0.453	0.062 ± 0.015	7	0.005 ± 0.001	3.64 ± 2.87	0.001 ± 0.000
Val313Pro	6.5	0.736 ± 0.059	7.794 ± 2.18	0.094 ± 0.027	6.5	0.201 ± 0.008	0.51 ± 0.16	0.394 ± 0.05
Val331Thr	6	0.292 ± 0.015	3.776 ± 0.881	0.079 ± 0.017			^a	

^aNo activity

the functional properties of these three positions in CsFDH and CtFDH. The determined kinetic constants are shown in Table 4 for wild-type CsFDH, CtFDH, and their mutants.

The CsFDH Val331Thr mutation had higher K_M and k_{cat} values, but low substrate affinity prevented an increase in catalytic efficiency (k_{cat}/K_M decreased from 0.107 to 0.079 s/mM). The same mutation on CtFDH, which is Val310Thr, had higher K_M and lower k_{cat} values, this mutation caused slightly decreasing in catalytic efficiency. Though these two mutations did not show activity at all in the CO₂ reduction reaction and CsFDH-Val331Thr had the lowest catalytic efficiency in oxidizing formate, but the maximum speed of its catalysed reaction can be reached with smaller amounts of formate than the others. A different mutation on the same position which is Val310Asn CtFDH mutation resulted in decreased k_{cat} and K_M values but was followed by a low catalytic efficiency due to a drastic decrease in the k_{cat} value.

Although the CsFDH-Asn312Phe mutation slightly increased the substrate affinity for formate, the catalytic efficiency (k_{cat}/K_M) of this mutant decreased to some degree, based on lowered k_{cat} values (Table 4).

The CsFDH-Val313Pro mutant showed decreased substrate affinity to formate (K_M 5.2 to 7.8 mM), whereas k_{cat} was slightly increased. It had comparable efficiency to the wild type in formate oxidation, while CO₂ reduction was four times as efficient as the wild type and two times as efficient as CsFDH-Asn312Phe. It also had more affinity towards hydrogen carbonate than the two other enzymes. Even though CsFDH had a very low activity for CO₂ reduction (0.8 mU/mg), it showed a dramatic increase over CtFDH in catalytic efficiency against HCO₃⁻, which was found to be the more promising FDH enzyme with its high activity for CO₂ reduction (34.6 mU/mg) (Choe et al. 2014, Aslan et al. 2017). It even resulted in better catalytic

efficiency in CO₂ reduction than the semi-rationally designed CtFDH mutant. The most promising mutant studied for CO₂ reduction, CtFDH-Gly93His/Ile94Ala, showed a slightly lower k_{cat}/K_M ratio (0.360 s⁻¹mM⁻¹) than the CsFDH-Val313Pro mutant (Çakar et al. 2020).

In addition, the site-directed mutations in CtFDH were made separately in four positions in the active site facing the substrate to study the possibility of modifying the reaction by changing the enzyme-substrate interactions. All three residues substituted with Ala caused a decrease in catalytic efficiency. The Ile94Ala and His312Ala CtFDH mutants had dramatically increased K_M and decreased k_{cat} for the forward reaction. The mutations Ile94Ala and His312Ala showed weakened binding of the substrate (K_M values of 20.85 mM and 7.18 mM, respectively). The Asn120Ala mutation also showed a loss of activity in formate oxidation. In addition to this dramatic effect, the reverse reaction still continues. The 2.7-fold higher K_M than its wild-type indicates that the mutant had decreased bicarbonate binding efficiency, while the catalysis rate was increased from 0.25 to 1.73/s at the same time. The mutation Ile94Ala showed the same effect for the reverse reaction: the K_M value increased from 0.35 to 1.734, while the k_{cat} value increased from 0.025 to 0.191. In contrast, the Ala mutation introduced to His312, another substrate-binding site, caused a complete loss of activity in the reverse reaction.

Molecular modelling of CsFDH and CtFDH

Despite CsFDH and CtFDH have ~53% sequence identities with PseFDH, the first shell active site residues of the three enzymes are conserved. Figures 2 and 3 highlight the substrate-binding pockets of CsFDH and CtFDH which are built by residues Pro97, Phe98,

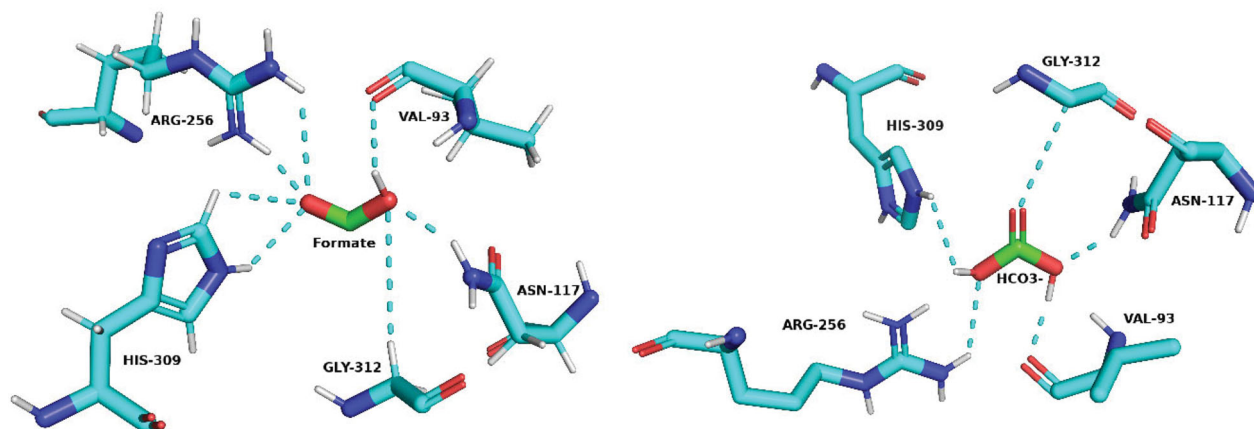


Figure 2. CsFDH active site residues are involved in the substrate-binding for formate oxidation and CO₂ reduction reactions.

Thr120, Gly124, Asn146, Val150, Arg284, Val309, His332, and Gly335 (according to *PseFDH* numberings).

Formate and hydrogen carbonate substrates were bound in the active site of *CsFDH* with H-bonds with Val93, Asn117, Arg256, His309 and Gly312 (Val93-O 2.5 Å, Asn117-1HD21 2.1 Å, Arg256-HH11 2.0 and HH21 3.1 Å, His309-HE1 3.0 and HE2 2.4 Å, Gly312-HA3 3.9 Å for formate and Val93-O 2.1 Å, Asn117-1HD2 2.1 Å, Arg256-2HH2 2.6 Å, His309-HE2 2.5 Å and Gly312-CA 3.5 Å for hydrogen carbonate, [Figure 2](#)).

The mutations Phe311Asn in *PseFDH* and Phe290Asn in *SoyFDH* similarly showed a decrease in catalytic efficiency due to their loss of affinity against formate (Alekseeva et al. [2012](#), Tishkov et al. [2015](#)). The mutations studied on *PseFDH*-Phe311 by Tishkov et al. revealed the formation of additional H-bonds. *PseFDH* wild-type forms only one H-bond in between Phe311 residue and nitrogen of Arg290 residue. However, this bond is also present in the replacement of Phe311 residue by Ser or Thr but disappears in mutants *PseFDH*-Phe311Asn. The same mutation on *SoyFDH* studied by Alekseeva et al. and Tishkov et al. resulted in increased K_M^{Formate} ([Table 5](#)). The reason for this is that Phe is a hydrophobic residue and contains a benzene ring, while Asn is an uncharged amino acid. It is thought to be that the Phe residue on the *CsFDH*-Asn312Phe mutant may cause a slight change in the folding of the protein, causing new H-bonds to form, positively affecting the substrate affinity.

In formate oxidation and CO₂ reduction, the *CsFDH* Val313Pro mutation enhanced the catalysis rate 1.3-fold and 18.3-fold respectively, while substrate-binding affinity decreased 1.5-fold and increased 28.4-fold respectively. Since the Val313Pro mutant had the highest catalytic efficiency on CO₂ reduction with 0.394/s.mM, it can be concluded that the hydrophobicity at this position is crucial for the appropriate orientation of His312 and accommodation of substrates (Aslan et al. [2017](#), Çakar et al. [2020](#), Yilmazer et al. [2020](#)).

According to the crystal structure (formate) and docking information (hydrogen carbonate) of *CtFDH*, the substrates were bound in the active site of *CtFDH* with H-bonds with Ile94, Asn120, Arg259, His312, and Gly315 (Ile94-O 2.7 Å and N 3.0 Å, Asn120-ND2 3.0 Å, R259-NH1 3.1 Å and NH2 3.4 Å, His312-CE1 3.1 Å and NE1 3.1 Å for formate and Ile94-HN 2.4 Å, Asn120-2HD2 2.2 Å, Arg259-1HH2 1.6 Å, His312-HE2 2.3 Å and Gly315-CA 3.5 Å for hydrogen carbonate, [Figure 3](#)).

Asn120 and Ile94 are the side chains in hydrogen-bonding distance from the substrate. They seem to coordinate the substrate into its place. The other side chains keeping the substrate in its place by hydrogen

bonds are Arg259 and His312 in *CtFDH* (Yilmazer et al. [2020](#)). These four residues form a network of hydrogen bonds staying tightly in place, thus controlling the exact positioning of the substrates ([Figure 3](#)). The Asn120Ala mutation possibly disrupts the H-bonding required for the exact positioning of the substrate at the enzyme active site, resulting in a loss of formate oxidation activity. Although there is one additional hydroxyl group in hydrogen carbonate compared to formate, the results show that the carbon dioxide reduction reaction still occurs, albeit with reduced efficiencies after the Asn120Ala mutation. In the Asn120Ala mutant, the formate molecule would move away from the catalytic position in the active site ([Figure 3](#)). This situation prevents the exact positioning of the formate carbon required for the forward reaction transfer of the hydride ion to the cofactor. However, the results show that the carbon dioxide molecule makes the reverse reaction less sensitive to the exact positioning of the substrate carbon. According to previous studies, mutations in these positions cause loosening of the tight control in the substrate positioning, giving flexibility to the conformation of the active site residues (Pala et al. [2018](#)). In our study, Asn120Ala, a change to a less bulky amino acid, can cause this effect. The flexibility means that the hydrogen carbonates can more easily move in their places. Decreasing of the binding in the mutant Asn120Ala increased the catalysis rate from 0.25 to 1.73/s like the Asn120Cys mutant ([Table 5](#)) (Pala et al. [2018](#)). Stronger binding of hydrogen carbonate could be the reason for the low catalysis rate by the wild type.

The Ile94Ala, another mutation in the substrate-binding site, showed similar effects to Asn120Ala in the reverse reaction but did not lose its activity in the forward reaction, although it was dramatically decreased. The formate molecule in the active site is kept in place by H-bonds to the main chain nitrogen of Ile94 (Yilmazer et al. [2020](#)). Although alanine is not very different from isoleucine, the dramatic increasing effect of the mutation on K_M value (3.7 to 20.8 mM) indicates that the H-bond between the formate and the Ala94 is disturbed. Nevertheless, the Ile94Ala mutant is active, with higher k_{cat} values than the wild type. In the reverse reaction, the smaller Alanine mutation introduces more space and more conformational flexibility to the active site as the Asn120Ala mutation does. Also, poorer bonding of the substrate can improve product release (Pala et al. [2018](#)), which may explain higher k_{cat} values.

Table 5. Functional effects of active site mutations in NAD⁺-dependent formate dehydrogenases.

Mutation	Source	Substrate/Cofactor	Results	Reference
Asn120Ala	CtFDH	Hydrogen carbonate	k_{cat} is increased 6.9-fold, K_M is increased 2.7-fold	This study
Asn120Cys	CmFDH	Hydrogen carbonate	k_{cat} and K_M are increased 7-fold.	Pala et al. (2018)
Asn119Tyr		Formate	K_M is decreased 1.4-fold	
Asn119His		Formate	k_{cat} is decreased 5-fold, K_M is decreased 2.2-fold	
Asn119Asp	CboFDH	Hydrogen carbonate/Formate	Not active with either substrate	Labrou and Rigden (2001)
Asn119His		NAD ⁺	K_M is increased 1250-fold, 0.1% activity, K_M is increased 78-fold	
Asn146Ser	PseFDH	Formate	K_M is increased 0.8-fold	Tishkov et al. (1996)
Asn146Cys	CsFDH	NAD ⁺	V_{max} is decreased 2-fold	
Asn146Ala		Formate	K_M is increased 60-fold	This study
Asn312Phe		NAD ⁺	K_M is increased 5.8-fold	
		Hydrogen carbonate	K_M is decreased 4-fold	
		Formate	k_{cat} is decreased 2-fold, K_M is decreased 1.3-fold	
Phe311Tyr	PseFDH	Formate	K_M is decreased 2.1-fold, thermostability is increased 1.6-fold	Tishkov et al. (2015)
Phe311Asn		NAD ⁺	K_M is increased 4.1-fold,	
		Formate	k_{cat} is decreased 1.4-fold, K_M is increased 2.5-fold, thermostability is decreased 2-fold	
Phe311Ser		NAD ⁺	K_M is increased 4.1-fold	
		Formate	k_{cat} is decreased 1.4-fold, K_M is increased 7.1-fold, thermostability is decreased 2-fold	
Phe311Asp		NAD ⁺	K_M is increased 5.6-fold	
		Formate	k_{cat} is decreased 1.8-fold, K_M is increased 9.3-fold, thermostability is increased 2.4-fold	
Phe290Ser	SoyFDH	NAD ⁺	K_M is decreased 1.5-fold	Alekseeva et al. (2012)
		Formate	k_{cat} is increased 1.4-fold, K_M is increased 2.7-fold, decrease in thermal stability	
Phe290Asn		Formate	K_M is increased 3-fold, thermal stability is increased	Alekseeva et al. (2012)
Phe290Asp		Formate	k_{cat} is increased 1.8-fold, K_M is increased 3.3-fold, thermal stability is highly increased	
Phe290Ala		NAD ⁺	K_M is decreased 1.5-fold	Kargov et al. (2015)
		Formate	k_{cat} is increased 1.4-fold, K_M is decreased 1.4-fold	
Phe290Tyr		NAD ⁺	K_M is decreased 1.2-fold,	
		Formate	k_{cat} is increased 1.2-fold, K_M is decreased 1.6-fold	
Phe290Gln		Formate	k_{cat} is increased 1.2-fold, thermal stability is increased 5-fold	
Phe290Glu		Formate	k_{cat} is increased 1.6-fold, and K_M is increased 1.9-fold	
Phe290Thr	CboFDH	Formate	k_{cat} is increased 1.4-fold	Slusarczyk et al. (2000)
Phe285Tyr		Formate	Thermal stability is increased 47-fold	
Val310Asn		Hydrogen carbonate	Not active with substrate	
	CtFDH	Formate	k_{cat} is decreased 13.3-fold, K_M is decreased 2.3-fold	This study
Val310Thr		Hydrogen carbonate	Not active with substrate	
		Formate	k_{cat} is decreased 4.7-fold, K_M is increased 1.8-fold	This study
Val331Thr	CsFDH	Hydrogen carbonate	Not active with substrate	
		Formate	k_{cat} is decreased 1.9-fold, K_M is decreased 1.4-fold	This study
His312Ala	CtFDH	Hydrogen carbonate	Not active with substrate	
		Formate	k_{cat} is decreased 18-fold, K_M is increased 2-fold	Pala et al. (2018)
His312Asp	CmFDH	Formate	K_M is decreased 1.3-fold	
His312Cys	PseFDH	Hydrogen carbonate/Formate	Not active with either substrate	Tishkov et al. (1996)
His312Ser		Hydrogen carbonate/Formate	Not active with either substrate	
His312Tyr		Hydrogen carbonate/Formate	Not active with either substrate	
His312Pse		Formate	Lost its activity through formate oxidation	
His312Ala	CboFDH	NAD ⁺	Does not affect the binding of NAD ⁺	Labrou and Rigden (2001)
His312Gln		Formate	0.1% activity, K_M is increased 10-fold	

Fraction analysis of wild-type and mutant FDHs with SDS-PAGE (Supplementary Figure S1).

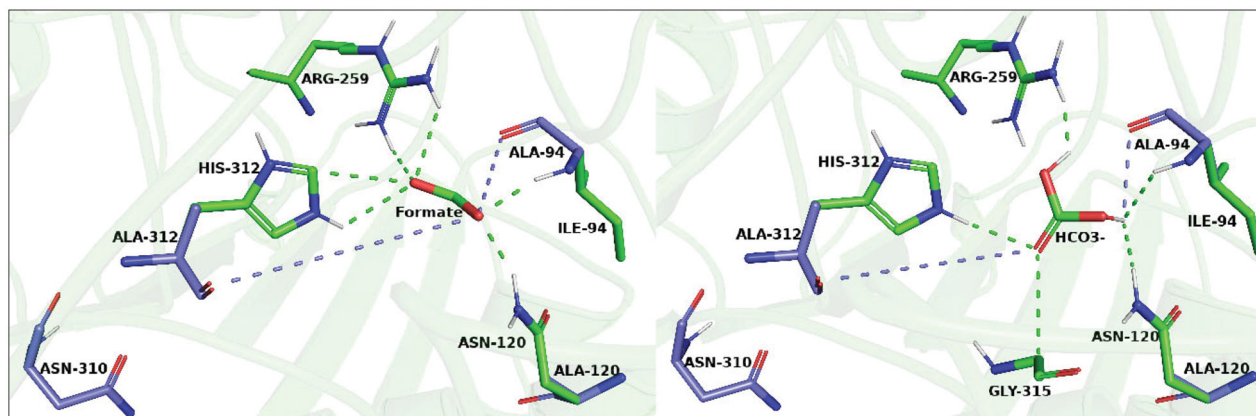


Figure 3. CtfDH active site residues are involved in the substrate-binding for formate oxidation and CO₂ reduction reactions. (Wild-type and mutant CtfDHs shown by green and blue sticks, respectively.).

The His312 mutation, one of the key conserved residues in the active site centre of FDHs, pairs with Gln288 to form a proton relay system required for acid–base catalysis. His is the best candidate for this task for both L- and D-specific dehydrogenase families at the active site of CtfDH. Since the His312 residue forms H-bonds with both substrates and silencing this residue with Ala substitution caused a dramatically abated K_M and k_{cat} values, His312 has to provide electrostatic interaction to achieve catalysis (Galkin et al. 2002). Mutations on this position in FDHs from different sources resulted in the loss of activity (Table 5).

CtfDH Val310 and CsFDH Val313 residues (which are strongly conserved among other FDHs as Thr (Figure 1), together with Asp283 (Asp280 for CsFDH) have van der Waals interactions on the side chain of His312 (His 309 for CsFDH). This key residue has H-bonds with both formate and hydrogen carbonate ions to keep the substrates in proper orientations.

The CtfDH Val310Asn mutation dramatically abated the catalysis rate for formate oxidation. Even though substrate affinity increased, a 13.3-fold decline in the catalysis rate resulted in a 5.7-fold decrease in catalytic efficiency. However, since the k_{cat} value was increased 3.6-fold for CO₂ reduction, catalytic efficiency did not change owing to the regression in substrate binding affinity.

Conclusion

In conclusion, we have examined the functional effects of active site mutations in CtfDH and CsFDH. These effects were clarified by pH and thermostability assay, measuring kinetics parameters (K_M , k_{cat}), and molecular modelling. Obtained results were compared with structurally equivalent positions which have been studied in the literature. The

present study indicates that the effect of mutations can cause small structural changes which create significant differences. Previous studies have shown that alanine mutation in the active site of CtfDH has a similar effect. Changing to a less-bulky amino acid disturbs the H bonding of the substrate and weaker binding provides flexibility for substrate release, which causes an increase in the catalytic rate. The Proline mutation at the 313 position of CsFDH shows very promising results on CO₂ reduction compared to the literature, even though this mutant is not directly involved in substrate binding. By this, it was understood that the orientation of the key residues with the amino acids having hydrophobic side chains is significant for the FDH catalysis. Results of this study enlighten the role of catalytic residues of CsFDH and provide a further understanding of the catalytic reaction mechanism of FDHs. Besides, this mutant enzyme would increase the possibility of FDH using for CO₂ reduction. FDHs are considered as unfavourable for electrochemical reduction of CO₂ due to their low catalytic rate constants (k_{cat}) for CO₂ reduction. However, the obtained mutant in this study and further engineering of FDHs in the light of this study can be integrated into electrochemical CO₂ reduction systems. FDHs are dimeric enzymes and can be easily inactivated depending on the process conditions by separating their subunits. Since the enzyme stability can be improved by immobilization to enable enzymes to be applicable in industrial processes, immobilization of these enzymes can be beneficial for reducing CO₂ on an industrial scale (Aivilova et al. 1985, Bolivar et al. 2007, Mateo et al. 2007, Fernandez-Lafuente 2009, Velasco-Lozano et al. 2017, Yildirim et al. 2019). Therefore, immobilized mutant enzyme might provide development of feasible and reusable CO₂ fixation processes.

Acknowledgements

The authors gratefully acknowledge the help and support of ETDAM (Enzyme Testing and Consultation Center, Gebze Technical University, Turkey).

Disclosure statement

We have no conflict of interest to declare.

Authors' contributions

BB has conceived and designed the study. BB, BY, MMÇ and YAW have predicted the mutations. KK, FŞ, YAW, BY, MMÇ, MB, IS, and MCB have carried out mutagenesis and characterization studies. MMÇ has carried out protein modelling. BB oversaw the project. The manuscript was written by KK, FŞ, YAW, BY, MMÇ, ESB and BB.

Funding

This work was partially supported by a grant from the TÜBİTAK [Grant number: 119Z155].

References

- Alekseeva AA, Serenko AA, Kargov IS, Savin SS, Kleymenov SY, Tishkov VI. 2012. Engineering catalytic properties and thermal stability of plant formate dehydrogenase by single-point mutations. *Protein Eng Des Sel.* 25(11):781–788.
- Alissandratos A, Kim HK, Easton CJ. 2013. Formate production through biocatalysis. *Bioengineered.* 4(5):348–350.
- Alissandratos A, Kim HK, Easton CJ. 2014. Formate production through carbon dioxide hydrogenation with recombinant whole cell biocatalysts. *Bioresour Technol.* 164: 7–11.
- Arnold K, Bordoli L, Kopp J, Schwede T. 2006. The SWISS-MODEL workspace: a web-based environment for protein structure homology modelling. *Bioinformatics.* 22(2): 195–201.
- Aslan AS, Valjakka J, Ruupunen J, Yildirim D, Turner NJ, Turunen O, Binay B. 2017. *Chaetomium thermophilum* formate dehydrogenase has high activity in the reduction of hydrogen carbonate (HCO₃⁻) to formate. *Protein Eng Des Sel.* 30(1):47–55.
- Avilova TV, Egorova OA, Ioanesyan LS, Egorov AM. 1985. Biosynthesis, isolation and properties of NAD-dependent formate dehydrogenase from the yeast *Candida methylifica*. *Eur J Biochem.* 152(3):657–662.
- Bassegoda A, Madden C, Wakerley DW, Reisner E, Hirst J. 2014. Reversible interconversion of CO₂ and formate by a molybdenum-containing formate dehydrogenase. *J Am Chem Soc.* 136(44):15473–15476.
- Bolivar JM, Wilson L, Ferrarotti SA, Fernandez-Lafuente R, Guisan JM, Mateo C. 2007. Evaluation of different immobilization strategies to prepare an industrial biocatalyst of formate dehydrogenase from *Candida boidinii*. *Enzyme Microb Technol.* 40(4):540–546.
- Çakar MM, Ruupunen J, Mangas-Sanchez J, Birmingham WR, Yildirim D, Turunen O, Turner NJ, Valjakka J, Binay B. 2020. Engineered formate dehydrogenase from *Chaetomium thermophilum*, a promising enzymatic solution for biotechnical CO₂ fixation. *Biotechnol Lett.* 42(11): 2251–2262.
- Choe H, Joo JC, Cho DH, Kim MH, Lee SH, Jung KD, Kim YH. 2014. Efficient CO₂-reducing activity of NAD-dependent formate dehydrogenase from *Thiobacillus* sp. KNK65MA for formate production from CO₂ gas. *PLoS One.* 9(7): e103111.
- Fernandez-Lafuente R. 2009. Stabilization of multimeric enzymes: strategies to prevent subunit dissociation. *Enzyme Microb Technol.* 45(6–7):405–418.
- Florides GA, Christodoulides P. 2009. Global warming and carbon dioxide through sciences. *Environ Int.* 35(2): 390–401.
- Galkin AG, Kutsenko AS, Bajulina NP, Esipova NG, Lamzin VS, Mesentsev AV, Shelukho DV, Tikhonova TV, Tishkov VI, Ustinnikova TB, et al. 2002. Site-directed mutagenesis of the essential arginine of the formate dehydrogenase active centre. *Biochim Biophys Acta.* 1594(1):136–149.
- Glueck SM, Gümüş S, Fabian WMF, Faber K. 2010. Biocatalytic carboxylation. *Chem Soc Rev.* 39(1):313–328.
- Hatrongjit R, Packdibamrung K. 2010. A novel NADP⁺-dependent formate dehydrogenase from *Burkholderia stabilis* 15516: screening, purification and characterization. *Enzyme Microb Technol.* 46(7):557–561.
- Hawkins AS, McTernan PM, Lian H, Kelly RM, Adams MWW. 2013. Biological conversion of carbon dioxide and hydrogen into liquid fuels and industrial chemicals. *Curr Opin Biotechnol.* 2013;24:376–384.
- Kargov IS, Kleymenov SY, Savin SS, Tishkov VI, Alekseeva AA. 2015. Improvement of the soy formate dehydrogenase properties by rational design. *Protein Eng Des Sel.* 28(6): 171–178.
- Karimäki J, Parkkinen T, Santa H, Pastinen O, Leisola M, Rouvinen J, Turunen O. 2004. Engineering the substrate specificity of xylose isomerase. *Protein Eng Des Sel.* 17(12):861–869.
- Kim S, Kim MK, Lee SH, Yoon S, Jung KD. 2014. Conversion of CO₂ to formate in an electroenzymatic cell using *Candida boidinii* formate dehydrogenase. *J Mol Catal B: Enzym.* 102:9–15.
- Labrou NE, Rigden DJ. 2001. Active-site characterization of *Candida boidinii* formate dehydrogenase. *Biochem J.* 354(2):455–463.
- Lamzin VS, Dauter Z, Popov VO, Harutyunyan EH, Wilson KS. 1994. High resolution structures of holo and apo formate dehydrogenase. *J Mol Biol.* 236(3):759–785.
- Lenz M, Fademrecht S, Sharma M, Pleiss J, Grogan G, Nestl BM. 2018. New imine-reducing enzymes from β -hydroxyacid dehydrogenases by single amino acid substitutions. *Protein Eng Des Sel.* 31(4):109–120.
- Leopoldini M, Chiodo SG, Toscano M, Russo N. 2008. Reaction mechanism of molybdoenzyme formate dehydrogenase. *Chemistry.* 14(28):8674–8681.
- Lu Y, Yi Jiang Z, Wei Xu S, Wu H. 2006. Efficient conversion of CO₂ to formic acid by formate dehydrogenase immobilized in a novel alginate-silica hybrid gel. *Catal Today.* 115(1–4):263–268.

- Maia LB, Moura I, Moura JGG. 2017. Molybdenum and tungsten-containing formate dehydrogenases: aiming to inspire a catalyst for carbon dioxide utilization. *Inorg Chim Acta*. 455:350–363.
- Mateo C, Palomo JM, Fernandez-Lorente G, Guisan JM, Fernandez-Lafuente R. 2007. Improvement of enzyme activity, stability and selectivity via immobilization techniques. *Enzyme Microb Technol*. 40(6):1451–1463.
- Pala U, Yelmazer B, Çorbacioğlu M, Ruupunen J, Valjakka J, Turunen O, Binay BBY, Çorbacioğlu M, Ruupunen J, Valjakka J, et al. 2018. Functional effects of active site mutations in NAD⁺-dependent formate dehydrogenases on transformation of hydrogen carbonate to formate. *Protein Eng Des Sel*. 31(9):327–335.
- Pettersen EF, Goddard TD, Huang CC, Couch GS, Greenblatt DM, Meng EC, Ferrin TE. 2004. UCSF Chimera – a visualization system for exploratory research and analysis. *J Comput Chem*. 25(13):1605–1612.
- Schiøtt B, Iversen BB, Madsen GKH, Larsen FK, Bruice TC. 1998. On the electronic nature of low-barrier hydrogen bonds in enzymatic reactions. *Proc Natl Acad Sci U S A*. 95(22):12799–12802.
- Shapovalov MV, Dunbrack RL Jr. 2011. A smoothed backbone-dependent rotamer library for proteins derived from adaptive kernel density estimates and regressions. *Structure*. 19(6):844–858.
- Slusarczyk H, Felber S, Kula MR, Pohl M. 2000. Stabilization of NAD-dependent formate dehydrogenase from *Candida boidinii* by site-directed mutagenesis of cysteine residues. *Eur J Biochem*. 267(5):1280–1289.
- Smith PK, Krohn RI, Hermanson GT, Mallia AK, Gartner FH, Provenzano MD, Fujimoto EK, Goeke NM, Olson BJ, Klenk DC. 1985. Measurement of protein using bicinchoninic acid. *Anal Biochem*. 150(1):76–85.
- Stierand K, Rarey M. 2010. Drawing the PDB: protein-ligand complexes in two dimensions. *ACS Med Chem Lett*. 1(9):540–545.
- Studier FW. 2005. Protein production by auto-induction in high density shaking cultures. *Protein Expr Purif*. 41(1):207–234.
- Tishkov VI, Goncharenko KV, Alekseeva AA, Kleymenov SY, Savin SS. 2015. Role of a structurally equivalent phenylalanine residue in catalysis and thermal stability of formate dehydrogenases from different sources. *Biochemistry (Mosc)*. 80(13):1690–1700.
- Tishkov VI, Matorin AD, Rojkova AM, Fedorchuk VV, Savitsky PA, Dementieva LA, Lamzin VS, Mezentzev AV, Popov VO. 1996. Site-directed mutagenesis of the formate dehydrogenase active centre: role of the His332-Gln313 pair in enzyme catalysis. *FEBS Lett*. 390(1):104–108.
- Tishkov VI, Popov VO. 2004. Catalytic mechanism and application of formate dehydrogenase. *Biochemistry (Mosc)*. 69(11):1252–1267.
- Tishkov VI, Popov VO. 2006. Protein engineering of formate dehydrogenase. *Biomol Eng*. 23(2-3):89–110.
- Trott O, Olson AJ. 2010. AutoDock Vina: improving the speed and accuracy of docking with a new scoring function, efficient optimization, and multithreading. *J Comput Chem*. 31(2):455–461.
- Velasco-Lozano S, Benítez-Mateos AI, López-Gallego F. 2017. Co-immobilized phosphorylated cofactors and enzymes as self-sufficient heterogeneous biocatalysts for chemical processes. *Angew Chem Int Ed Engl*. 56:771–775.
- Wu H, Tian C, Song X, Liu C, Yang D, Jiang Z. 2013. Methods for the regeneration of nicotinamide coenzymes. *Green Chem*. 15(7):1773–1789.
- Yildirim D, Alagöz D, Toprak A, Tükel S, Fernandez-Lafuente R. 2019. Tuning dimeric formate dehydrogenases reduction/oxidation activities by immobilization. *Process Biochem*. 85:97–105.
- Yilmazer B, Isupov MN, De Rose SA, Bulut H, Benninghoff JC, Binay B, Littlechild JA. 2020. Structural insights into the NAD⁺-dependent formate dehydrogenase mechanism revealed from the NADH complex and the formate NAD⁺ ternary complex of the *Chaetomium thermophilum* enzyme. *J Struct Biol*. 212(3):107657.
- Yuan M, Kummer MJ, Minteer SD. 2019. Strategies for bioelectrochemical CO₂ reduction. *Chemistry*. 25(63):14258–14266.